DEVELOPMENTS OF ELECTRON CYCLOTRON EMISSION SPECTROSCOPY AND MICROWAVE REFLECTOMETRY ON LHD

T. TOKUZAWA,[a]* K. KAWAHATA,[a] Y. NAGAYAMA,[a] S. INAGAKI,[b] P. C. DE VRIES,[c] A. MASE,[d] Y. KOGI,[d] Y. YOKOTA,[d] H. HOJO,[e] K. TANAKA,[a] A. EJIRI,[f] R. O. PAVLICHENKO,[g] S. YAMAGUCHI,[h] T. YOSHINAGA,[a] D. KUWAHARA,[i] Z. SHI,[j] H. TSUCHIYA,[a] Y. ITO,[a] S. HIROKURA,[a] S. SUDO,[a] A. KOMORI,[a] and LHD EXPERIMENT GROUP[a]

[a]*National Institute for Fusion Science, Toki 509-5292, Japan*
[b]*Research Institute for Applied Mechanics, Kyushu University, Fukuoka 816-8580, Japan*
[c]*Euratom/UKAEA Fusion Association, Culham Science Centre, Abingdon OX14 3EA, United Kingdom*
[d]*Art Science and Technology Center for Cooperative Research, Kyushu University, Kasuga 816-8560, Japan*
[e]*Plasma Research Center, University of Tsukuba, Tsukuba 305-8577, Japan*
[f]*Graduate School of Frontier Sciences, The University of Tokyo, Kashiwa 277-8561, Japan*
[g]*Institute of Plasma Physics, National Science Center, Kharkov Institute of Physics and Technology 1, Akademicheskaya St., Kharkov, 61108, Ukraine*
[h]*Faculty of Engineering Science, Kansai University, Osaka 564-8680, Japan*
[i]*Tokyo Institute of Technology, Tokyo 152-8550, Japan*
[j]*Graduate University for Advanced Studies, Toki 509-5292, Japan*

Received August 19, 2009
Accepted for Publication December 2, 2009

Several types of microwave diagnostics, in the category of electron cyclotron emission (ECE) spectroscopy and reflectometry, have been developed on the Large Helical Device (LHD). Since LHD has a complicated magnetic configuration, the polarization effects have been studied for optimization of the microwave passive and active diagnostics. It was found that if the density is sufficiently high, the effect of mode conversion is negligible and the local polarization angle can be estimated as the angle at the plasma boundary. Three types of ECE spectroscopy, which are the heterodyne radiometer, the Michelson spectrometer, and the grating polychromator, have been optimized and operated routinely in order to measure radial profiles of electron temperature and its fluctuations in the frequency range 50 to 500 GHz. Several types of microwave reflectometers have also been utilized for measurements of the electron density profile and fluctuations. Two ultrashort pulsed radar reflectometers for density profile measurements, a V-band frequency-hopping reflectometer for density fluctuation profile measurements, and a fixed-frequency three-channel homodyne reflectometer for the interlock system of the neutral beam injection have been routinely operated. Also, an advanced diagnostic, which uses an imaging technique, has been developed to study the two- or three-dimensional structure of temperature and density fluctuations.

KEYWORDS: *LHD, ECE, reflectometer, microwave diagnostics*

I. INTRODUCTION

Microwave diagnostics have been well utilized for the plasma confinement studies for a long time by passive or active means. Of the former, one application is the electron cyclotron emission (ECE) measurement for the electron temperature measurements. The microwave reflectometer for the electron density measurements is an example of the latter. Figure 1b shows the spatial profiles of the characteristic frequencies of the Large Helical Device[1] (LHD) plasma with the typical plasma parameters $[B_0 = 2.75\ \mathrm{T}, n_e(0) = 10^{20}\ \mathrm{m}^{-3}]$. It is found that most of

*E-mail: tokuzawa@nifs.ac.jp

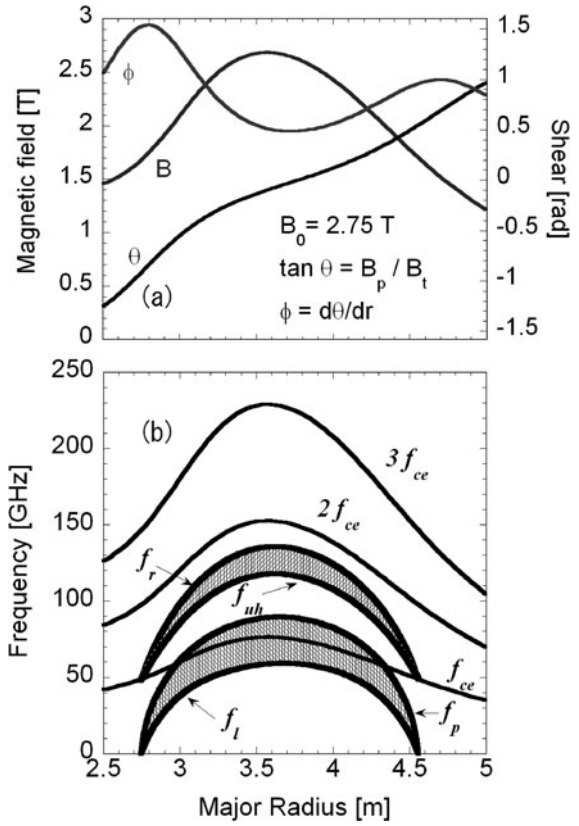

Fig. 1. (a) Magnetic field configuration in the equatorial plane of the horizontal cross section when the magnetic axis is 3.60 m and the magnetic field strength B_0 is 2.75 T. The magnetic field strength, the shear $\theta = a\tan(B_{pol}/B_{tor})$, and its derivative ϕ are plotted. (b) First, second, and third harmonics of ECE frequencies, including microwave cutoffs and resonances: (f_{ce}) electron cyclotron, (f_r) right cutoff, (f_l) left cutoff, (f_{uh}) upper hybrid. Here, the density profile is assumed to be $n_e(r) = 10^{20}[1 - (r/a)^2]\ \mathrm{m}^{-3}$.

the characteristic frequencies are located in the microwave region in LHD.

The ECE measurement is a powerful diagnostic for measuring the local electron temperature of magnetized confinement plasmas, since the ECE frequency is proportional to the magnetic field, which is different at each position in the plasma. However, the analysis of the ECE spectrum from LHD is not as straightforward as in the case of tokamak plasmas. The magnetic field strength in LHD is a nonmonotonic function of the radius in the sight line of the ECE diagnostic antenna and is characterized by a large shear, as shown in Fig. 1a. The shear in LHD is of order unity at the plasma edge. Such a large shear yields a coupled propagation of the ordinary (O-) and extraordinary (X-) polarization modes, yielding mode conversion and polarization rotation.[2] The detailed numerical and experimental analyses of the ECE polarization need to be performed. This knowledge is quite useful for the other microwave applications. ECE antennas have been installed both on the inner side and on the outer side ports in the equatorial plane in LHD. Each antenna is connected to a Michelson interferometer,[3,4] high- and low-frequency heterodyne radiometers,[5] and a grating polychrometor[6] (GPC) via 80 m of corrugated waveguide. As shown in Fig. 1b, the first-harmonic ordinary mode cannot propagate in the main part of the plasma column because of the presence of the plasma cutoff region. The second-harmonic extraordinary mode, which radiates as a blackbody in almost the whole region of the plasma column, is able to travel through the plasma up to the density $n_e(0) = 1.7 \times 10^{20}\ \mathrm{m}^{-3}$ without plasma cutoff effects.

Microwave reflectometry is a radar technique for density profile and density fluctuation measurements by using the cutoff phenomenon in a plasma. Because the measured time of flight (TOF) through a plasma involves information about the change of refractive index, we can obtain the local information about electron density using this TOF value. Also, the TOF measurements have the advantage that they can distinguish between O- and X-polarization modes by the time lag. We initially developed and installed a moderate pulsed radar reflectometer.[7] This reflectometer used a 1-ns pulse modulated microwave and measured the oscillation of the cutoff layer. The line averaged density could also be measured by this system used as a delayometer.[8] However, for precise spatial resolution measurements, wider band frequency components are needed. Hence, we started development of an ultrashort pulsed radar reflectometer.[9–11]

For density fluctuation measurements, several other microwave reflectometers have been applied in LHD. In particular, to measure the radial distribution of fluctuation, the frequency-hopping reflectometer[12] has been applied. Another application of the reflectometer is with the interlock apparatus.[13] In this technique, the reflected signal from the plasma is used to show the existence of the corresponding cutoff layer.

Recently, a new application, the microwave imaging system,[14] has been developed. It is an advanced diagnostics system for measuring the two-dimensional (2-D) or three-dimensional (3-D) image of the electron temperature and/or density profile and these fluctuations.

In this paper, we describe the polarization effect in a helical plasma in Sec. II, the ECE systems in Sec. III, the reflectometer systems in Sec. IV, and the imaging diagnostics in Sec. V, where some experimental results are also given. Section VI summarizes the work.

II. POLARIZATION EFFECT

The plasma is a refractive medium for microwaves. The refractive index is a complex function depending on the local magnetic field strength and plasma parameters. Because O- and X-modes have different refractive indices, their propagations differ too.

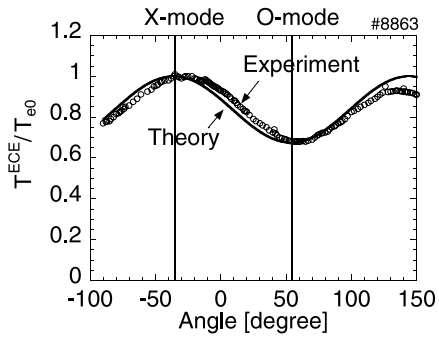

Fig. 2. The ratio of the radiation intensity and the electron temperature versus the angle in the laboratory frame. The theoretical curve is obtained as the intensity of the O-mode ECE fit to the observation. The X-mode intensity is calibrated by the Thomson scattering.

LHD has a specific magnetic field configuration (see Fig. 1a). It has a maximum in the center and large shear. In the case of ECE measurements, each frequency, emitted from a different position, will have its own polarization under a different angle in the laboratory frame. Furthermore, the shear causes the propagation of the two polarization modes to be coupled.[2] The coupled wave equations were solved numerically.[15,16] It is found that the mode conversion is negligible at densities $n_e > 0.5 \times 10^{19}$ m^{-3}. Also, the polarization of the ECE wave rotates following the rotation of the magnetic field vector when the density is efficiently high. Therefore, the ECE polarization can be determined at the plasma edge, where the electron density sharply drops to zero. This is a good assumption in LHD. Usually, the ECE spectrometer detects one polarization component. Here, let α be the angle of the detection system, θ the angle of the magnetic field at the plasma edge, T_X the intensity of the X-mode ECE, and T_O the intensity of the O-mode ECE. The intensity T of the ECE wave is written as $T = T_O \cos^2(\alpha - \theta) - T_X \sin^2(\alpha - \theta)$.

Experiments were performed in order to verify the polarization of the ECE spectrum. During a long-pulse plasma discharge with central electron density $n_e(0) =$ 1.5 to 1.8 $\times 10^{19}$ m^{-3} and central electron temperature $T_e(0) = 4.2$ to 3.7 keV, the universal polarization rotator of the ECE system was rotated. In this condition, the plasma is optically thick ($\tau > 5$) for the X-mode ECE. Figure 2 shows the ratio of the radiation intensity to the electron temperature versus the angle in the laboratory frame. The theoretical curve[15] is also plotted. A nice match between the measured and calculated curves is found.

The polarization rotation is therefore useful, because for each spectral component, each O- and X-mode wave will have a specific orientation in the laboratory frame. Hence, X- and O-modes can be distinguished in LHD.

III. ECE DIAGNOSTICS

Four kinds of ECE instruments have been installed and routinely operated to provide the electron temperature profile information. The characteristics of each instrument are summarized in Table I.

Since the magnetic field is a nonmonotonic function of radius in LHD, it is impossible to measure the full temperature profile along the major radius by using a single receiving antenna. Therefore, we have installed antennas both on the inner side and on the outer side ports in the equatorial plane. Figure 3 shows a schematic diagram of the ECE diagnostic system. The outer and the inner port antennas are designed to gather radiation with a vertical spatial resolution on the midplane of at least 10 and 3 cm, respectively. Two instruments, a GPC and a Michelson spectrometer, are connected to the outside antenna via some 80 m of 63.5-mm-diameter corrugated waveguides. The other instruments, 70- and 140-GHz heterodyne radiometers, are connected to the inside antenna. These antenna combinations can be arranged by reconnecting the waveguide. The waveguide is designed to transfer microwaves from 50 to 220 GHz with low loss. The total transmission loss of this system was measured to be ~3 dB. Three kinds of notch filters, which have band-stop characteristics at the harmonic frequencies 84, 82.6, and 77 GHz, are installed to eliminate noise signals from electron cyclotron heating (ECH). Each notch

TABLE I

Characteristics of ECE Diagnostics on the LHD

	Michelson Spectrometer	Grating Polychromator	70-GHz Radiometer	140-GHz Radiometer
Time resolution	25 ms	1 μs	1 μs	1 μs
Frequency range	50 to 500 GHz	105 to 148 GHz	53 to 87 GHz	106 to 158 GHz
Frequency resolution	4.0 GHz	2.6 GHz at 150 GHz	1 GHz	1 to 2 GHz
Number of channels	1	14	32	32
Detector	InSb	InSb	Schottky diode	Schottky diode

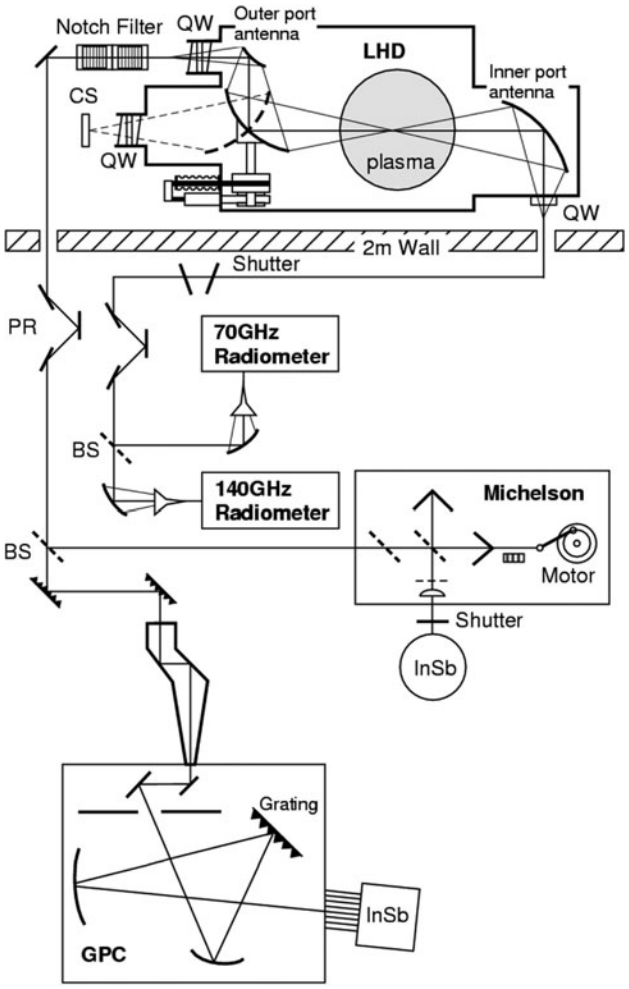

Fig. 3. Schematic diagram of the ECE diagnostic system in LHD.

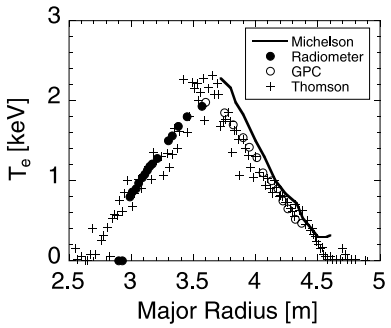

Fig. 4. Examples of calibrated ECE spectra obtained by the Michelson, the 70-GHz radiometer, and the GPC. The electron temperature profile measured by the Thomson scattering is also shown.

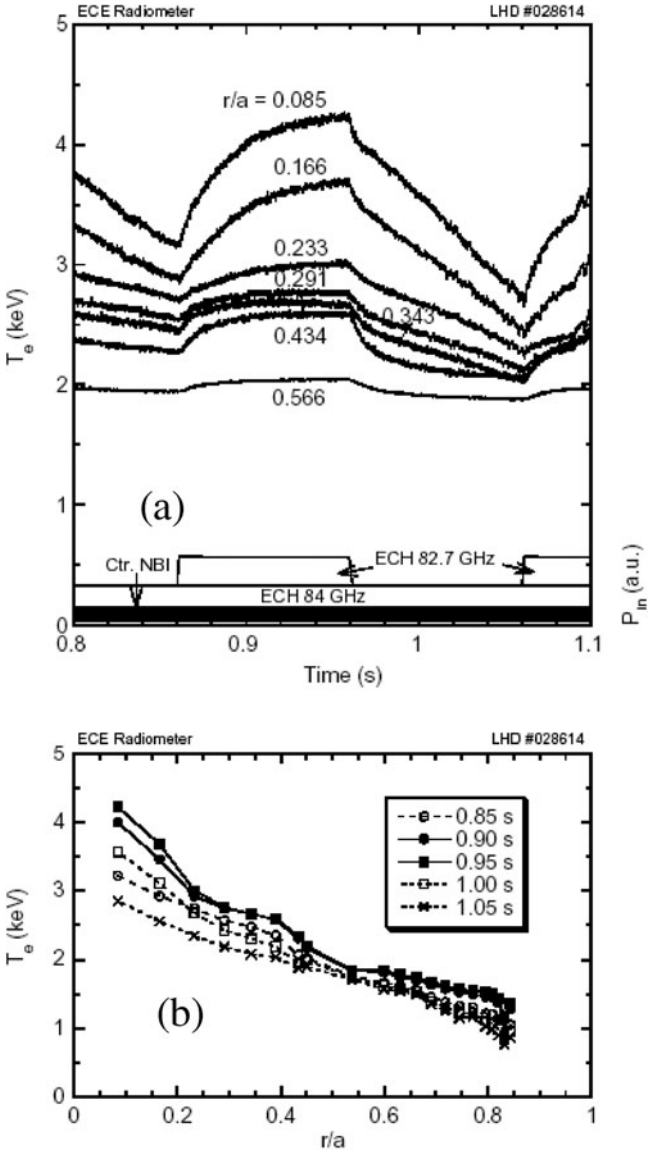

Fig. 5. (a) Temporal behavior of the electron temperature measured by ECE from different radial positions of the plasma with the ITB. The ITB is created by the injection of 84-GHz ECH into the NBI-heated plasma. The modulated ECH of 82.7 GHz is injected to investigate thermal transport in the ITB. (b) Evolution of the T_e profile of the plasma with the ITB measured by ECE. (From Ref. 5.)

filter attenuates by 30 dB with a full width of ~1 GHz and negligible insertion loss.

By calibrating the ECE spectrometers, the electron temperature can be measured. In LHD, the ECE, which is collected by the outer antenna and is detected by the fast-scanning Michelson spectrometer, can be absolutely calibrated using the calibration sources, which are indicated as CS in Fig. 3. The temperature of the calibration source is set at 800 K. Since the magnetic field strength has a peaked profile, both sides of the electron temperature profile can be measured by the ECE spectrometers. Examples of electron temperature profiles, which are measured by the Michelson, the radiometer, the GPC, and

also Thomson scattering, are shown in Fig. 4. In this case, the radiometer and the GPC are cross-calibrated to the Thomson scattering measurements in different shots. So by cross-calibrating to the Michelson, the GPC and radiometers are useful for measuring the electron temperature profile on LHD.

In particular, the excellent features of the heterodyne radiometer, high spatial and temporal resolutions, are favorable for the study of fast phenomena such as transport transitions,[5] magnetohydrodynamic activity,[17] nonlocal heat transport,[18,19] etc. Figure 5 shows examples of the radiometer measurements.[5] ECE signals are emitted from different radial positions of the plasma when the internal transport barrier (ITB) is formed around $r/a \sim 0.3$. In LHD, the ITB is created by the injection of highly localized 84-GHz ECH at the center of the neutral beam injection (NBI)–heated plasma. In this plasma discharge, additional ECH at 82.7 GHz with 100% modulated power is also injected to investigate the heat transport inside and outside the transport barrier. The evolution of the electron temperature profile is depicted in Fig. 5b, showing the location of the transport barrier around $r/a \sim 0.3$. After injection of the modulated ECH, the ECE signals located near the center of the plasma ($r/a < 0.3$) gradually increase until the end of the ECH pulse and then gradually decrease after the ECH power is switched off. This is in contrast to the time behavior of the signals located outside the ITB, which show a much smaller change. It can be clearly seen that the decay time constant of the electron temperature after switching off the modulated ECH power is quite long (~100 ms) in the core plasma compared with that (20 to 30 ms) outside the ITB. This indicates that a thermal transport barrier is formed around $r/a \sim 0.3$.

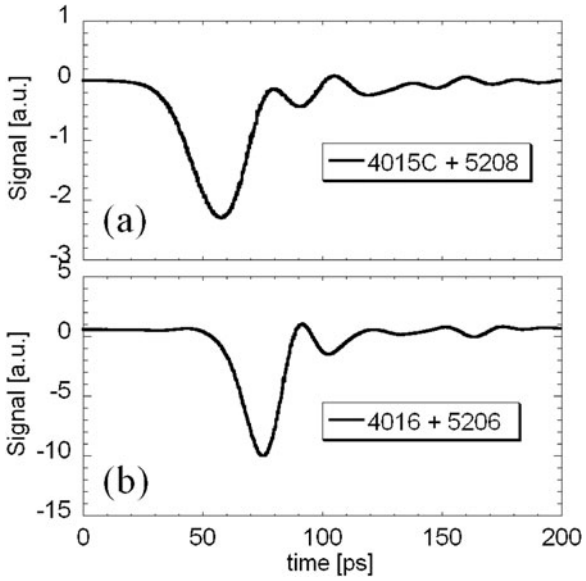

Fig. 6. Waveforms of an impulse from the impulse generator of (a) PSPL-4015C (FWHM of 23 ps) and (b) PSPL-4016 (FWHM of 18 ps).

IV. REFLECTOMETER

Several types of microwave reflectometers[7,9–13] have been installed on LHD for various purposes. Here, we show three of the reflectometer systems.

IV.A. Ultrashort Pulsed Radar Reflectometer

To measure the density profile by using reflectometry, broadband frequency components have to be utilized. The ultrashort pulsed radar reflectometer (UPRM) is one promising method used to measure electron density profiles without perturbing the plasma. In this diagnostic, an impulse waveform voltage is used as the source. Since the frequency bandwidth of the impulse source is in inverse relation to the temporal pulse width, we can employ a source with a broadband frequency range. The density profiles can be reconstructed by collecting the TOF signal of each frequency component of the impulse reflected from each corresponding cutoff layer.

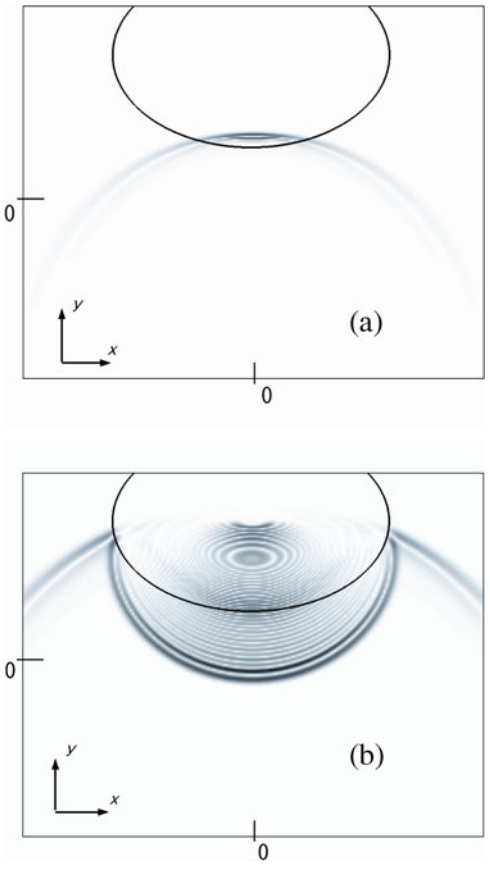

Fig. 7. Snapshot of (a) the incident pulse (E_z) and (b) the reflected wave (E_z). (From Ref. 20.)

In LHD, two UPRM systems have been developed using two different impulse generators. One source is a Picosecond Pulse Labs (PSPL) model 4015C impulse-generator with a model 5208 impulse-forming network, which generates a voltage impulse with an amplitude of −2.2 V and full-width at half-maximum (FWHM) of 23 ps. The other source is a model 4016 impulse generator with a model 5206 impulse-forming network, which generates an impulse with an amplitude of −2.0 V and FWHM of 18 ps. These impulse waveforms are shown in Fig. 6.

We first performed a simulation study of the UPRM to investigate its suitability and efficiency for helical plasmas.[20] A 2-D simulation model is used and Maxwell's equations are solved. The numerical scheme is based on the finite-difference time domain method. For a helical magnetic field configuration, an analytic model obtained in Ref. 21 is assumed. Here, the toroidal magnetic field is in the z direction, and the poloidal magnetic field is in the x-y plane. We assume a Gaussian pulse with the pulse width of 30 ps as the incident pulse, which is launched from the lower boundary in the y direction. Figure 7a shows a snapshot of the electric wave field E_z of the incident pulse, and Fig. 7b shows the reflected wave field E_z from the LHD plasma. We note that E_z can be regarded to be approximately O-mode, since the toroidal field is much stronger than the poloidal field. For the reflected wave, we see that E_z is almost symmetric with respect to the central line of $x = 0$, similar to O-mode. It is found that UPRM can work successfully for helical plasmas.

Figure 8 shows the UPRM system for a TOF type of measurement using an 18-ps impulse as the source.[9] The repetition rate of the pulse is usually 100 kHz. This system currently has 28 channels, consisting of 2 channels in the X-band, 24 channels in the Ka-band, and 2 channels in the U-band. The TOF obtained as a function of the frequency is utilized for the density profile measurement. Since the measured points are discrete and limited, the TOF profile needs to be interpolated. The position of the corresponding cutoff layer, that is, the density profile, is obtained by Abel inversion. Figure 9 shows the evolution of reconstructed density profile measured by this reflectometer.

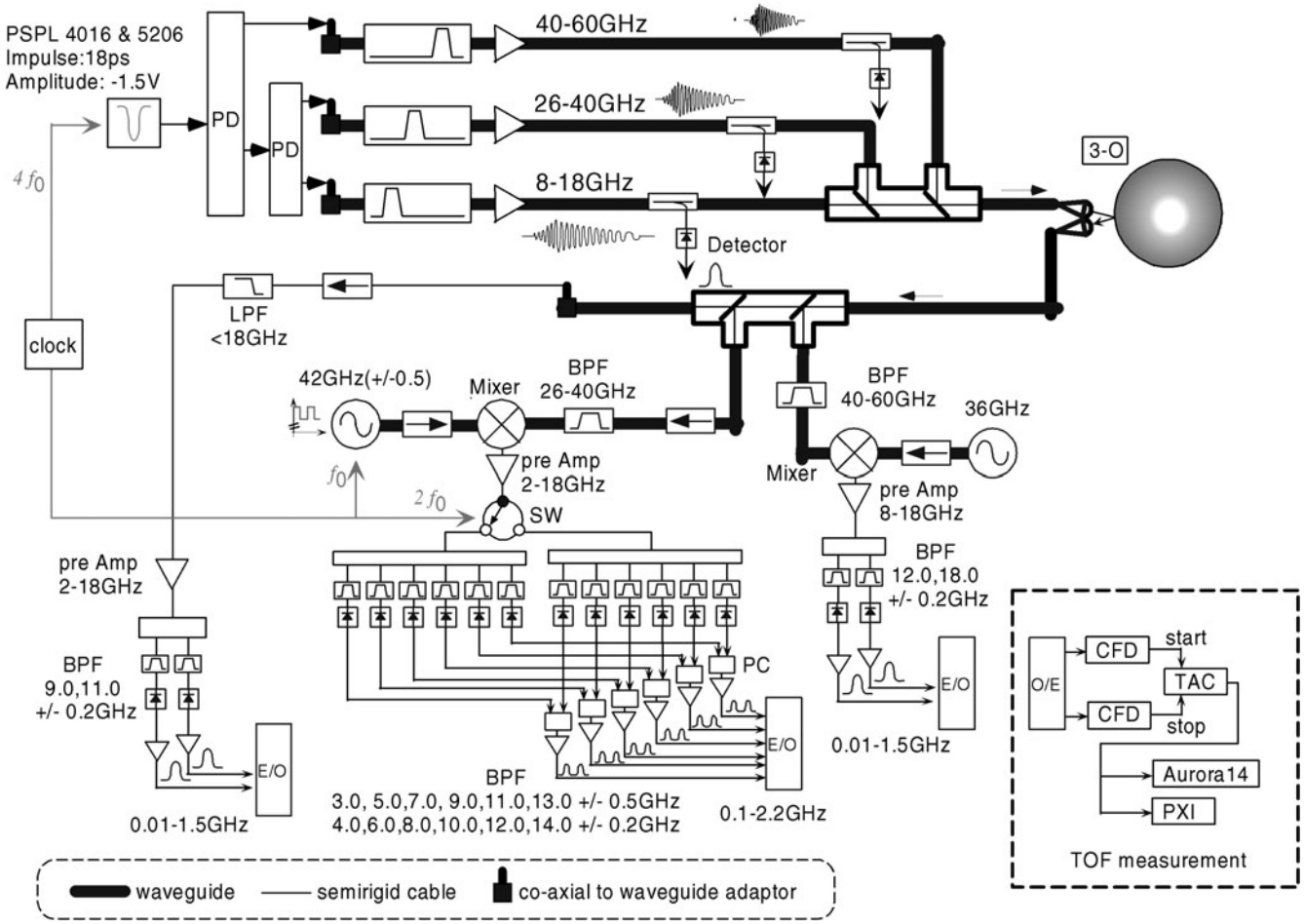

Fig. 8. Schematic view of TOF type of UPRM system. (From Ref. 9.)

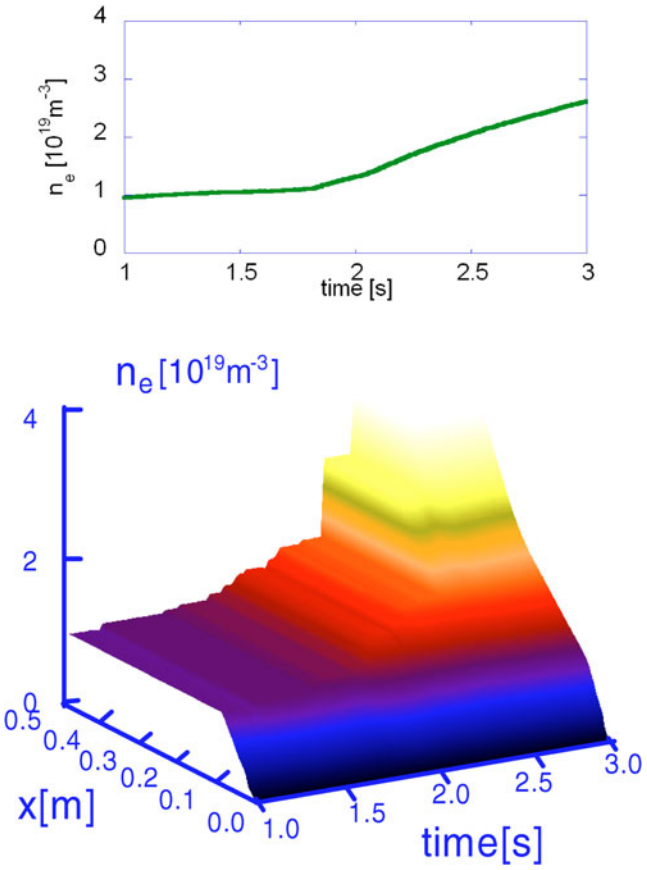

Fig. 9. Evolution of (a) averaged density and (b) density profile.

We have developed another UPRM system.[10,11] This system is used with the signal record analysis (SRA) method.[22] To attain precise reconstruction of the profile, detection channels over the whole frequency range are necessary. The SRA method is an efficient and precise solution to this problem. Figure 10 shows the schematic of this UPRM system. The pulse width, height, and repetition rate of the impulse are 22 ps, −3 V, and 1 MHz, respectively. The frequency range of 18 to 40 GHz is utilized for the probe beam. The reflected waves are directly recorded by a high-speed digitizing scope at 250 GHz and analyzed by the SRA method for density reconstruction. In addition, a remote control system, as shown in Fig. 10, has been introduced to this UPRM system utilizing the Super-SINET (Ref. 23) between the National Institute for Fusion Science (NIFS) and Kyushu University. The bandwidths of the main backbone and branch line are 10 and 1 gigabits/s, respectively. The control client can operate the control server by using this network. A general-purpose interface bus (GPIB) card is installed in the control server. The remote console, which has a graphical user interface, is used to control the instruments of the USPRM via GPIB. The entire system, including adjustment of supply voltage fed to amplifiers

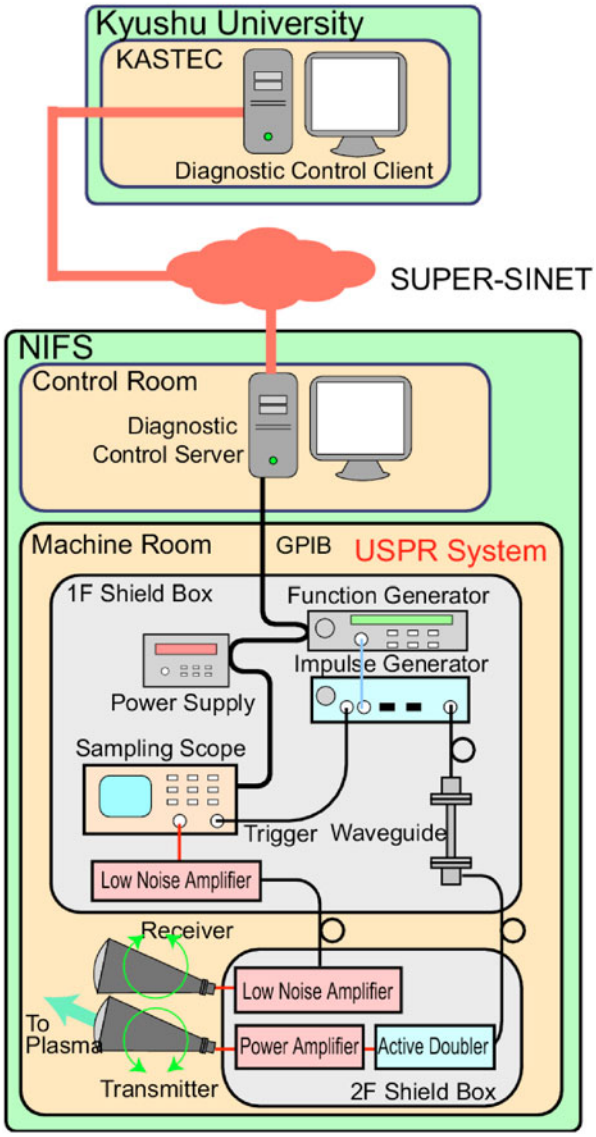

Fig. 10. Schematic of the SRA UPRM system, including the remote control system.

and doubler, timing control of the impulse, antenna position, data acquisition, and monitoring, can be operated from the remote site. A TV conference system via the Super-SINET is also installed in order to communicate with the NIFS control room.

IV.B. Frequency-Hopping Reflectometer

To measure the radial distribution of fluctuations in a wide range, a reflectometer needs many probing frequency components. When the plasma condition can be assumed to be steady state during a frequency scanning period, the radial profile can be measured by using a wideband frequency source system. In this operation, the

source frequency is swept step by step in the whole frequency range. This type of frequency sweep is referred to as frequency hopping. The step width and the number of steps are arranged by the characteristic time of the measured fluctuation frequency.

A schematic of a frequency-hopping V-band reflectometer system[12] is shown in Fig. 11. A microwave synthesizer is used as a source with a low phase noise. The output frequency increases step by step. The typical value of each frequency sweeping time is 20 ms and the number of steps is 20. Also, for direct *I-Q* phase measurement, single-sideband (SSB) frequency modulation is utilized. The output signals of the *I-Q* demodulator, which are described by $A\cos\phi$ and $A\sin\phi$, are acquired by a real-time data acquisition system based on a compact PCI digitizer and are sampled at a typical rate of 1 MHz during the whole plasma discharge. By evaluating the system performance, the phase perturbation level is ~1/30 fringe. In the case of $L_n = 50$ mm, this value corresponds to $\delta n/n \sim 10^{-4}$.

In Fig. 12, we show a preliminary experimental result of this hopping system for the radial distribution measurement of Alfvén eigenmodes. The experiment is carried out on a discharge where the axial magnetic field strength is 2.0 T, the averaged electron density is $<0.4 \times 10^{19}$ m^{-3}, and three tangential neutral beams are injected with constant power. While the plasma condition is mostly steady state and the fluctuation frequency stays constant, the probe frequency is swept from 48 to 72 GHz in 1-GHz steps of 20-ms duration. We can see continuous coherent frequency components of about 120 kHz in this probe frequency range. The toroidal mode number of this coherent fluctuation is $n = 1$ as measured by the magnetic probe. The radial fluctuation profile of the frequency components of 110 to 130 kHz is shown in Fig. 12c. Here, the calculated displacement ξ is also plotted. It can be seen that this mode is large around $\rho = 0.3$. The calculated shear Alfvén spectra are also shown in Fig. 12b. The frequency gap of ~120 kHz is located near $\rho = 0.25$. It is in good agreement with the measured profile data.

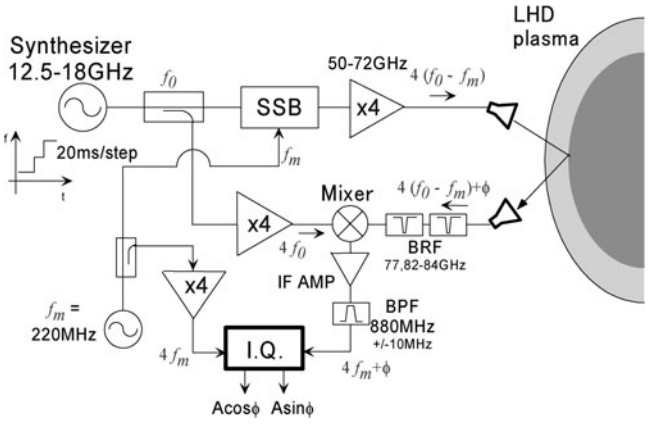

Fig. 11. Schematic of the V-band frequency-hopping microwave reflectometer. f_0 is carrier frequency (12.5 to 18 GHz), f_m is modulation frequency (220 MHz), and ϕ is plasma fluctuation component. (From Ref. 12.)

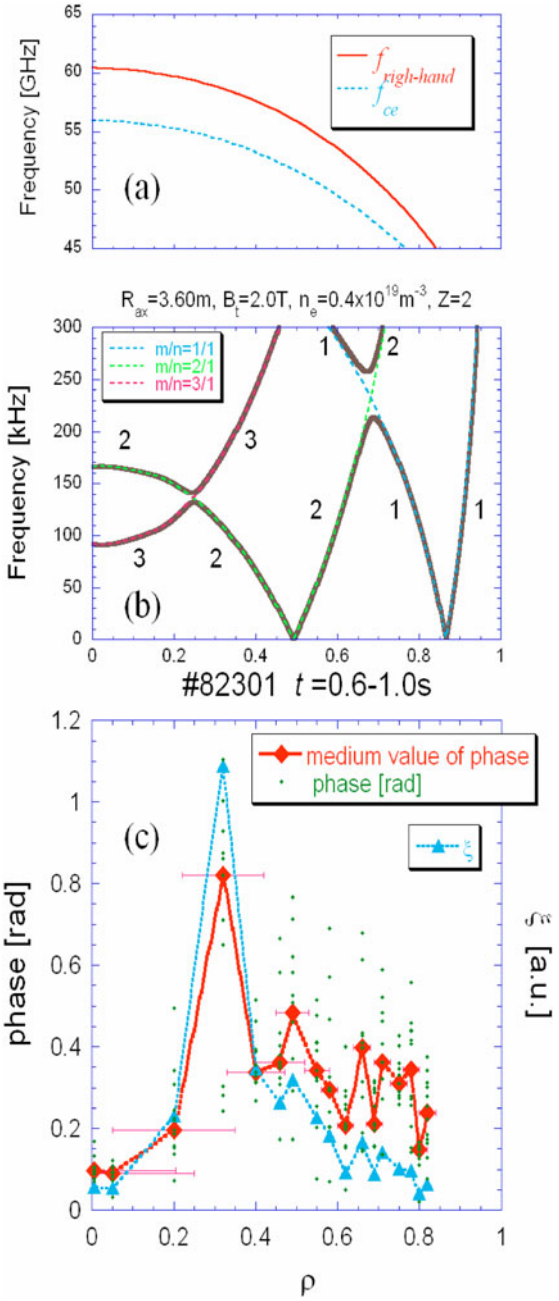

Fig. 12. (a) Radial profiles of the right-hand X-mode cutoff frequency (solid line) and electron cyclotron frequency (dotted line) for a discharge in LHD. (b) Radial profile of the shear Alfvén spectra of $n = 1$. Each number expresses the poloidal mode number. (c) The amplitude of phase fluctuation (dots), with frequency components of 110 to 130 kHz, and medium value at each radial position (thick line with diamonds) and calculated radial displacement (thin line with triangles).

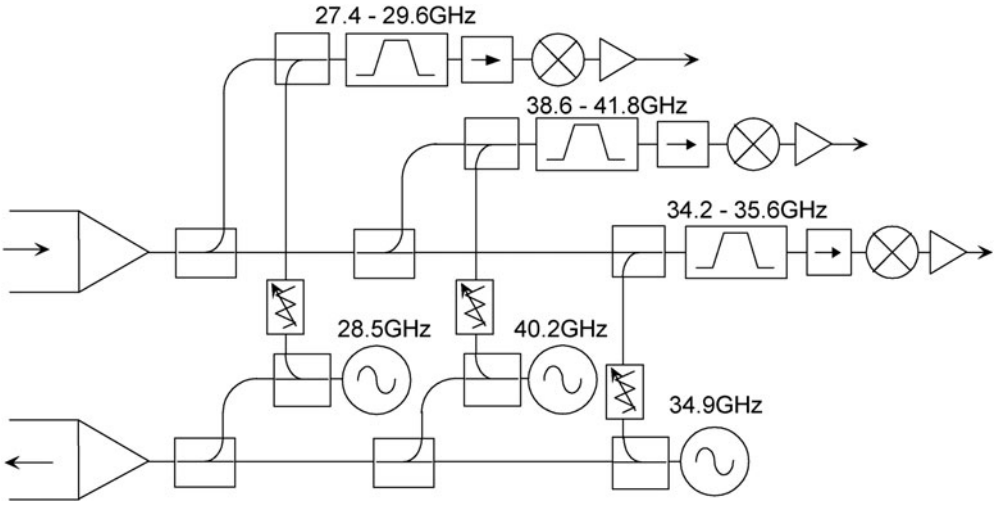

Fig. 13. Schematic diagram of transmission and detection components of a three-channel homodyne interlock reflectometer.

IV.C. Homodyne Reflectometer for NBI Interlock

Reflectometry is utilized not only for a physics study but also as a system control tool. Here, we explain an example of the application of the reflectometer signal to the device control.

A reliable NBI interlock system is required in magnetically confined plasma devices. In the case of LHD, the armor tiles at the NBI dump are designed to endure 100-ms exposure at full NBI power (7.5 MW) with no target plasma. If the NBI continues after plasma termination, the full neutral beam power is deposited on the vessel wall, which can cause serious damage. The NBI shine-through ratio is more than 50% at densities $<1 \times 10^{19}$ m^{-3}. Therefore, the NBI has to be stopped when the density decreases below this value.

Among several possible diagnostics for the interlock source, a microwave reflectometer is selected. It is expected to be a simple and reliable density monitor. Figure 13 shows a schematic diagram of transmission and detection components of the density interlock reflectometer.[13] The system has three channels, with frequencies at 28.5, 34.9, and 40.2 GHz, which correspond to O-mode cutoff densities of 1.0, 1.5, and 2.0×10^{19} m^{-3}, respectively. The amplitude level of the fluctuation signal is used as the source for the interlock.

Figure 14 shows an example of a discharge in which the reflectometer interlock was activated. A signal of 34.9 GHz is used as an interlock source in this plasma discharge. The NBI pulse was programmed to occur during $t = 0.4$ to 9.4 s, but the plasma suddenly terminated at $t = 4.1$ s because of a radiation collapse. Between $t = 0.9$ and $t = 3.78$ s, the line average density increased gradually at almost constant radiation power. At $t = 3.6$ s, the radiation power started to increase and the diamagnetic stored energy started to decrease. At $t = 3.78$ s, the

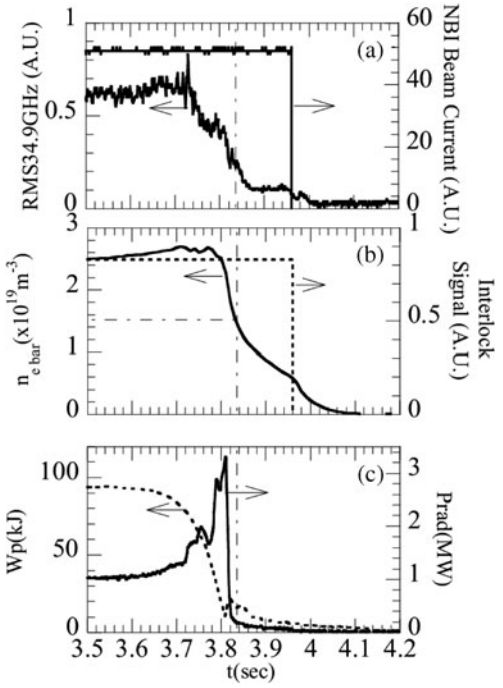

Fig. 14. Time trace of (a) 34.9-GHz rms signal and NBI current, (b) line averaged density and interlock signal, and (c) stored energy and radiation power. Thin vertical dotted lines indicate the timing when the averaged density reaches 1.5×10^{19} m^{-3}, which is a 34.9-GHz O-mode cutoff density.

average density started to decrease. As shown in Figs. 14a and 14b, the rms value of the 34.9-GHz reflected signal and the line average density follow almost the same trace. Presently, the interlock level is determined empirically, and the lower interlock level corresponding to the lower

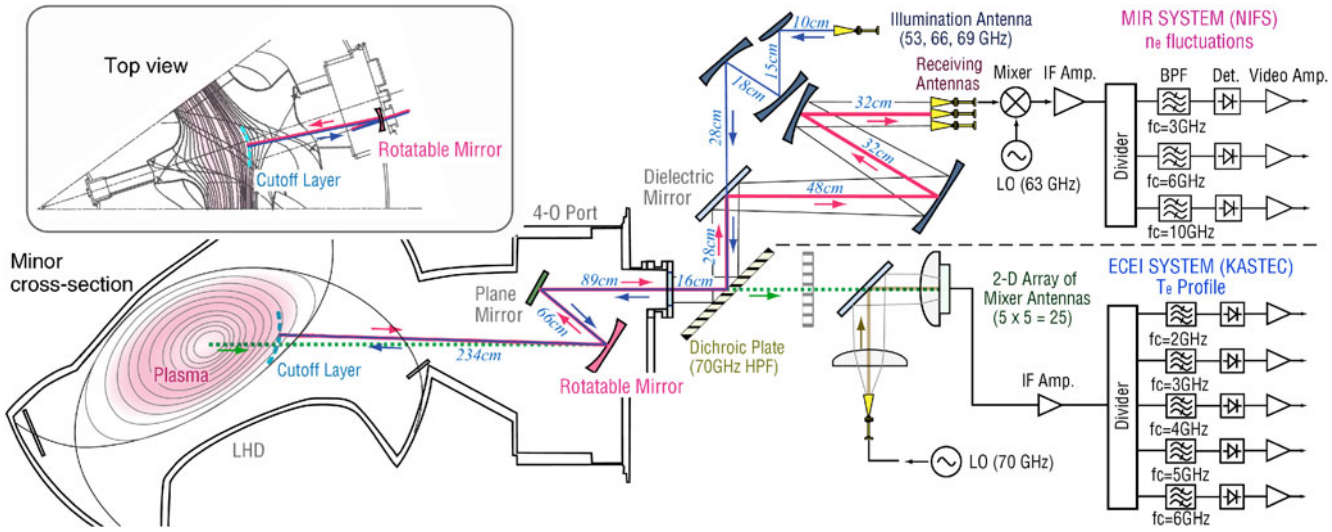

Fig. 15. Schematic of the microwave imaging system with combined MIR and ECEI in LHD. (From Ref. 25.)

interlock density is usually used. Therefore, the interlock signal is useful for protecting the NBI armor tiles and LHD vacuum vessel.

V. TEST INSTRUMENTS FOR IMAGING CONCEPT

Here, we show an advanced microwave diagnostic, that is, microwave imaging. In LHD, combined microwave imaging diagnostic techniques of ECE imaging[24] (ECEI) and microwave imaging reflectometry[25] (MIR) are under development to obtain a 2-D/3-D image of turbulences and instabilities with good temporal and spatial resolution.

A schematic view of the current combined microwave imaging system is shown in Fig. 15. Combined MIR/ECEI systems share the same optical imaging system in vacuum, and their beam paths are separated by an 8-mm-thick dichroic plate, which works as an optical high-pass filter. The dichroic plate has a clear cutoff feature at 70 GHz, so that it can separate the operational frequency range for MIR (50 to 70 GHz) and for ECEI (70 to 140 GHz). Since the optical layout enables the measurement of the cross correlation between the MIR and ECEI signals at the same location, we get information on both the density and temperature fluctuations simultaneously.

Using standard heterodyne techniques, an imaging system would require a large number of high-functional millimeter wave components to construct a high-resolution image. We have employed cost-effective millimeter integrated circuit (MIC) technology to construct an optimized system.[26] The initial experiment of ECEI with the MIC detector array has been carried out in the condition where the electron density and temperature in the core region attained values of 2.2×10^{19} m^{-3} and 3.75 keV, respectively. The temporal behavior of the output signal is almost in agreement with that of the electron temperature. In the near future, we will obtain 2-D/3-D images of both temperature and density fluctuation by this combined imaging diagnostic system.

VI. SUMMARY

Microwave technology has been making rapid progress. Improved plasma diagnostics have been developed by using some of these new techniques. In LHD, several types of microwave diagnostics, namely, ECE spectroscopy and reflectometry, have been installed and operated routinely for measuring the electron temperature and density profiles as well as fluctuations of T_e and n_e with high temporal and spatial resolution by using each system's strong point. Also, the advanced imaging diagnostics will be of practical use for plasma physics studies such as turbulence phenomena in the near future.

ACKNOWLEDGMENTS

This work is supported by budgets of the National Institute for Fusion Science (Nos. NIFS10ULPP008, NIFS10ULHH010, NIFS07KCHH012, NIFS07KCHH014, and NIFS-ULBB501). Also, it is supported in part by KAKENHI (Nos. 18035015, 18686075, 20026010, 22360394, and 22017007). The authors are grateful to the LHD operation group for their excellent technical support.

REFERENCES

1. O. MOTOJIMA et al., "Overview of LHD," *Nucl. Fusion*, **43**, 1674 (2003).

2. I. FIDONE and G. GRANATA, "Propagation of Electromagnetic Waves in a Plasma with a Sheared Magnetic Field," *Nucl. Fusion*, **11**, 133 (1971).

3. Y. NAGAYAMA, S. INAGAKI, H. SASAO, P. VRIES, Y. ITO, K. KAWAHATA, K. NARIHARA, and I. YAMADA, "Overview of ECE Diagnostics on LHD," *Fusion Eng. Des*., **53**, 201 (2001).

4. Y. NAGAYAMA, K. KAWAHATA, S. INAGAKI, T. MORISAKI, and K. NARIHARA, "Electron Cyclotron Emission Diagnostics for Helical Plasma in the Large Helical Device," *IEEE Trans. Plasma Sci.*, **32**, 1716 (2004).

5. K. KAWAHATA, Y. NAGAYAMA, S. INAGAKI, and Y. ITO, "Broadband Electron Cyclotron Emission Radiometry for the Large Helical Device," *Rev. Sci. Instrum*., **74**, 1449 (2003).

6. K. KAWAHATA, P. C. DEVRIES, Y. NAGAYAMA, S. INAGAKI, T. TOKUZAWA, K. TANAKA, and S. SASAO, "The 14-Channel Grating Polychromator for ECE Measurements in LHD," *Rev. Sci. Instrum*., **72**, 387 (2001).

7. T. TOKUZAWA, K. KAWAHATA, R. PAVLICHENKO, K. TANAKA, and A. EJIRI, "Pulsed Radar Reflectometry on the LHD," *Rev. Sci. Instrum*., **72**, *1*, 328 (2001).

8. A. J. H. DONNE, S. H. HEIJNEN, and C. A. J. HUGENHOLTZ, "Pulsed Radar Reflectometry and Prospects for Fluctuation Measurements," *Fusion Eng. Des*., **34–35**, 72 (1997).

9. T. TOKUZAWA, K. KAWAHATA, Y. ITO, K. TANAKA, and I. YAMADA, "Development of Plasma Diagnostics System Using an Impulse Waveform Voltage," *Plasma Fusion Res*., **3**, 018 (2008).

10. A. MASE et al., "Remote Experiment of Ultrashort-Pulse Reflectometry for Large Helical Device Plasmas," *Rev. Sci. Instrum*., **77**, 10E916 (2006).

11. Y. YOKOTA, A. MASE, Y. KOGI, L. BRUSKIN, T. TOKUZAWA, and K. KAWAHATA, "Measurement of Edge Density Profiles of Large Helical Device Plasmas Using an Ultrashort-Pulse Reflectometer," *Rev. Sci. Instrum*., **79**, 056106 (2008).

12. T. TOKUZAWA, A. EJIRI, K. KAWAHATA, K. TANAKA, and Y. ITO, "V-Band Frequency Hopping Microwave Reflectometer in LHD," *Rev. Sci. Instrum*., **79**, 10, 10F109 (2008).

13. K. TANAKA, A. EJIRI, Y. ITO, K. KAWAHATA, T. TOKUZAWA, M. OSAKABE, and Y. TAKEIRI, "Homodyne Reflectometer for Neutral Beam Injection Interlock on Large Helical Device," *Rev. Sci. Instrum*., **77**, 10E912 (2006).

14. Y. NAGAYAMA, and A. MASE, "Microwave Imaging Diagnostics," *J. Plasma Fusion Res*., **81**, *5*, 337 (2005).

15. P. C. DE VRIES, K. KAWAHATA, Y. NAGAYAMA, H. SASAO, S. INAGAKI, and K. NAGASAKI, "The Polarization of Electron Cyclotron Emission Spectra in the Large Helical Device," *Phys. Plasmas*, **7**, 3707 (2000).

16. P. C. DE VRIES, K. KAWAHATA, Y. NAGAYAMA, S. INAGAKI, H. SASAO, and Y. ITO, "Electron Cyclotron Emission Measurements by Means of a Grating Polychromator on the Large Helical Device," *Fusion Eng. Des*., **53**, 185 (2001).

17. Y. NAGAYAMA et al., "Sawtooth Oscillation in Current-Carrying Plasma in the Large Helical Device," *Phys. Rev. Lett*., **90**, 205001 (2003).

18. S. INAGAKI et al., "Observation of Reduced Heat Transport Inside the Magnetic Island O Point in the Large Helical Device," *Phys. Rev. Lett*., **92**, 055002 (2004).

19. S. INAGAKI et al., "Abrupt Reduction of Core Electron Heat Transport in Response to Edge Cooling on the Large Helical Device," *Plasma Phys. Control. Fusion*, **48**, A251 (2006).

20. H. HOJO, A. FUKUCHI, A. ITAKURA, and A. MASE, "Full-Wave Simulations on Ultrashort-Pulse Reflectometry for Helical Plasmas," *Rev. Sci. Instrum*., **75**, 3813 (2004).

21. T. WATANABE and H. AKAO, "Symmetry Relation for Helical Plasma," *J. Plasma Fusion Res*., **73**, 186 (1997).

22. L.G. BRUSKIN, A. NASE, A. YAMAMOTO, and Y. KOGI, *Plasma Phys. Control. Fusion*, **43**, 1333 (2001).

23. Science Information Network, http://www.sinet.ad.jp/

24. A. MASE et al., "Electron Cyclotron Emission Imaging on a Large Helical Device," *Rev. Sci. Instrum*., **74**, 1445 (2003).

25. S. YAMAGUCHI, Y. NAGAYAMA, Z. SHI, R. PAVLICHENKO, S. INAGAKI, Y. KOGI, and A. MASE, "Microwave Imaging Reflectometry in LHD," *Plasma Fusion Res*., **2**, S1038 (2007).

26. Y. KOGI, T. SAKODA, A. MASE, N. ITO, S. YAMAGUCHI, Y. NAGAYAMA, and K. KAWAHATA, "Development of ECE Imaging System on LHD," *Plasma Fusion Res*., **2**, S1032 (2007).